

# Modeling of A Microfluidic Electrochemical Cell for the Electro-reduction of CO<sub>2</sub> to CH<sub>3</sub>OH

Yosra Kotb<sup>1, 2</sup>, Seif-Eddeen K. Fateen<sup>1, 3</sup>, Jonathan Albo<sup>4</sup>, Ibrahim Ismail<sup>1, 2</sup>

<sup>1</sup> Chemical Engineering Department, Faculty of Engineering, Cairo University, 12613 Giza, Egypt

<sup>2</sup> Renewable Energy Engineering Program, University of Science and Technology, Zewail City, 12588 Giza, Egypt

<sup>3</sup> Environmental Engineering Program, University of Science and Technology, Zewail City, 12588 Giza, Egypt

<sup>4</sup> Department of Chemical & Biomolecular Engineering, University of Cantabria, Avda. Los Castros s/n, 39005 Santander, Spain

## Abstract

This study focuses on developing a mathematical model for the electrochemical reduction of CO<sub>2</sub> into CH<sub>3</sub>OH in a microfluidic flow cell. The present work is the first attempt to model the electro-reduction of CO<sub>2</sub> to alcohols, which is a step forward towards the scale up of the process to industrial operation. The model features a simple geometry of a filter press cell in which the steady state isothermal reduction takes place. All significant physical phenomena occurring inside the cell are taken into account, including mass and charge balances and transport, fluid flow and electrode kinetics. The model is validated and fitted against experimental data and shows an average error of 20.2%. The model quantitatively demonstrated the dominance of the

hydrogen evolution over the  $\text{CH}_3\text{OH}$  production and the limitations imposed on the process due to the mass transfer of the reactants to the cathode, especially  $\text{CO}_2$ . Also, the model shows that based on the flow pattern of  $\text{CH}_3\text{OH}$ , more conductive membrane materials could be used to decrease the potential drop around the membrane in order to improve the process performance.

As CO<sub>2</sub> emissions account for about 65% of the greenhouse gases emissions, this gas is considered to be the most prevalent cause for the global warming crisis.<sup>1</sup> About three-quarters of these emissions are due to fossil fuels burning on which the world relies as a supply for the ever growing energy demands. To limit the environmental damage, decreasing CO<sub>2</sub> emissions has become a worldwide concern that is being increasingly explored amid the scientific community.

There are different available technological options to mitigate CO<sub>2</sub> emissions from the atmosphere. One of these approaches is CO<sub>2</sub> Capture and Sequestration (CCS), whereby a concentrated stream of CO<sub>2</sub> is produced, transported and stored in places isolated from the atmosphere like deep oceans or underground.<sup>2,3</sup> Three pathways exist to achieve the CCS process: post-combustion capture, oxy-fuel combustion and pre-combustion capture. Although this technology can contribute to the reduction of CO<sub>2</sub> emissions from the atmosphere, the implementation of such technology still face several issues to solve. Among these issues are the economics, the regulatory framework and safety related to the unknown long term environmental impacts of CO<sub>2</sub> storage and the possible leakages.<sup>4,5</sup>

A more attractive option to CCS is the so-called CO<sub>2</sub> capture and utilization (CCU)<sup>5-7</sup>. CO<sub>2</sub> can be utilized as a raw material for producing bulk chemicals, polymers and fine chemicals. The utilization also incorporates the physical use of CO<sub>2</sub> as a solvent or in the oil and gas industry for enhanced oil recovery (EOR) and enhanced gas recovery (EGR).<sup>5,6</sup> Utilizing CO<sub>2</sub> as a building block to produce fine chemicals is much more appealing than CCS, because it produces a valuable product such as fuels that are usually produced from hydrocarbons. Pairing this useful CO<sub>2</sub> conversion into chemicals with a renewable energy source, such as solar or wind energy, would provide a means of storing the energy of these intermittent renewable energy sources.

This conversion process would generate carbon neutral fuels to be used at a large scale for electricity generation.

Among the available technologies for CO<sub>2</sub> conversion into value-added chemicals, the electrochemical route appears to be convenient since it can be conducted at mild reaction conditions to generate relatively high energy density fuels and valuable products.<sup>6,7</sup>

Electrochemical reduction of CO<sub>2</sub> involves applying a potential between two electrodes to allow CO<sub>2</sub> to be transformed into reduced forms such as CO,<sup>8,9</sup> formic acid/formate,<sup>10,11</sup> methane,<sup>12,13</sup> ethylene,<sup>14,15</sup> or alcohols.<sup>16–18</sup>

From the possible reduction products of the electrochemical utilization of CO<sub>2</sub>, CH<sub>3</sub>OH is considered to be one of the most promising alternatives.<sup>6,19</sup> CH<sub>3</sub>OH is a green fuel that has a high energy density by weight and by volume. In addition, its room temperature storage does not require high pressures. It is used as a raw material for many chemicals including dimethyl ether, gasoline, formaldehyde, etc.<sup>7,19</sup> Most importantly, it can be used directly in the present energy converting systems like internal combustion engines and fuel cells.<sup>19,20</sup> These advantages lead scientists to define the concept of “methanol economy”, in which CH<sub>3</sub>OH is produced in a carbon neutral cycle and then used as a renewable fuel or as a feedstock to almost all the chemicals now derived from fossil fuels.

Most of the studies in the field of electrochemical reduction of CO<sub>2</sub> adopted the experimental path to determine suitable electrodes, catalysts selective to a certain product, applied potential, and reaction mechanisms.<sup>8,21</sup> To better understand the pathways for CO<sub>2</sub> electro-reduction into various products, comprehensive modeling studies directly linked to experimental work must be developed. Previous modeling cases include the model of laboratory scale-up of continuous

trickle bed reactor for CO<sub>2</sub> electro-reduction to potassium formate.<sup>22</sup> The model used four fitted kinetic parameters and was able to simulate the reactor performance over a wide range of conditions with maximum error in formate current efficiency of  $\pm 20\%$  compared to the experimental work. Another model for the CO<sub>2</sub> reduction to CO on flat gold and silver electrodes in aqueous KHCO<sub>3</sub> and NaClO<sub>4</sub> solutions adequately agreed with experimental data.<sup>21</sup> Co-electrolysis of CO<sub>2</sub> and H<sub>2</sub>O in a solid oxide electrolyzer cell for syngas production was also modeled in another study to characterize the performance of the cell.<sup>23</sup> The model took into account the water-gas shift reaction in the cathode and good agreement was observed between modeling results and experimental data from literature. This model was followed by several models for syngas production from co-electrolysis of CO<sub>2</sub> and H<sub>2</sub>O in solid oxide electrolyzer cells.<sup>24–26</sup>

As for microfluidic electrolytic cells (MEC), which have been experimentally **proven to be efficient tools** to enhance the electrochemical reduction of CO<sub>2</sub>,<sup>27</sup> there is still a lack of modeling work to fully understand the system.<sup>28</sup> A first numerical model for CO<sub>2</sub> electro-reduction to formic acid in a MEC was presented by Wang et al.<sup>29</sup> In this model, the mass transfer and electrochemical characteristics at the cathode side were studied and good agreement was observed between the simulation and experimental results. It was concluded that the limiting factors to the cell performance are the low diffusivity of CO<sub>2</sub> in the porous electrodes, the competing hydrogen reaction and the dilution effect of H<sub>2</sub>. Another model was developed by Wu et al. for CO<sub>2</sub> electro-reduction to CO in a MEC.<sup>8</sup> This model studied charge, mass and momentum transport and electrochemistry at both the cathode and the anode. The model is validated against experimental data and shows good agreement especially at high cell potentials.

As discussed, previous modeling work of CO<sub>2</sub> electro-reduction in MEC accounted for products like formic acid or CO. Up to date, there are no modeling studies involving the electrochemical conversion of CO<sub>2</sub> into alcohols, which lately gained interest among the scientific community. In this study, a numerical model for the electrochemical reduction of CO<sub>2</sub> to CH<sub>3</sub>OH in a MEC is considered. This model is a steady state, isothermal model which considers species mass transport, charge transport and different electrode reactions. The model is validated with reported experimental data of CO<sub>2</sub> electro-reduction to CH<sub>3</sub>OH at Cu<sub>2</sub>O/ZnO-based electrode.<sup>30</sup>

### Microfluidic Electrolytic Cell

The schematic for modeling and geometric parameters of the MEC simulated in this study are obtained from the work of Albo et al.<sup>30</sup> as shown in Figure 1. Briefly, it consists of a cathode layer, two aqueous electrolyte channels, a Nafion 117 membrane and an anode plate. A 0.5 M aqueous potassium bicarbonate solution flows as anolyte and the same solution saturated with CO<sub>2</sub> enters as catholyte with a flow rate of 20 ml/min for each channel. The cathode is a Cu<sub>2</sub>O-ZnO gas diffusion electrode (1:1 weight ratio) and the anode is platinized titanium. The Nafion membrane separates the two electrolyte flow channels. The electrolyte enters from one side and exists on the other side along with the products of the reactions.

[FIGURE 1]

For the electrochemical reduction of CO<sub>2</sub> to CH<sub>3</sub>OH studied here, the dissolved CO<sub>2</sub> reacts at the cathode side by Reaction 1 to produce CH<sub>3</sub>OH. Reaction 2 is the byproduct reaction producing CO. The competing HER, which has a reduction potential only 20 mV less than that of CO<sub>2</sub> reduction, takes place at the cathode by Reaction 3. CH<sub>3</sub>OH, CO and H<sub>2</sub> are produced at the cathode side and come out with the flowing electrolyte. The CO reaction was added in an

attempt to bring the model results closer to experimental ones, as CO is believed to be one of the major byproducts obtained on copper electrode surfaces.<sup>7,31</sup>



While at the opposite electrode, the oxygen evolution Reaction 4 takes place to balance the electrons consumed at the cathode.



## Mathematical modeling

### Model assumptions

The developed steady-state model contained the following assumptions.

- 1) As there are no significant variations across the cell width, the model is developed in 2 dimensions to reduce the computational time. This assumption has been used and justified in previous literature.<sup>8,32</sup>
- 2) The temperature was not allowed to vary as the temperature variation across the channels is relatively small, especially due to the low current density and the presence of a liquid-flowing electrolyte, which is a good thermal conductor.<sup>8,33</sup>
- 3) The kinetic rates of electrochemical reactions can be described by forms of Butler-Volmer equation, which has been widely used to describe the kinetics of electrochemical reactions.<sup>34,35</sup>

4) Catalyst layer is treated as an infinitely thin film interface in contact with the electrolyte.

This assumption is made to reduce the complexity of the model. Modeling the porous gas diffusion electrodes would increase the simulation constraints and ambiguity.<sup>36</sup>

### Governing equations

The model takes into account species balance and transport, electronic and ionic charge balance and electrochemical **reaction** kinetics at both the cathode and anode. The following sections illustrate the governing equations inside each domain.

#### Electrolyte channels

In both electrolyte channels, species mass continuity is applicable. The equation is given as:

$$\nabla \cdot \mathbf{N}_i = R_i \quad (1)$$

where  $\mathbf{N}_i$  is the species mass flux and  $R_i$  is the reaction source/sink term. Since the electrochemical reactions are limited to the electrode surface, **the  $R_i$  term is set to 0 inside the electrolyte channels.**

The species flux is computed with Nernst-Planck equation which considers the species transport by diffusion, electric migration and convection.<sup>37,38</sup> The flux is determined as follows:

$$\mathbf{N}_i = -D_i \nabla c_i - z_i u_{m_i} F c_i \nabla \Phi_{l,e} + \mathbf{u} c_i \quad (2)$$

where  $i$  applies to each species ( $\text{H}^+$ ,  $\text{OH}^-$ ,  $\text{K}^+$ ,  $\text{HCO}_3^-$ ,  $\text{CO}_3^{2-}$ ,  $\text{CO}_2$ ,  $\text{H}_2$ ,  $\text{CH}_3\text{OH}$ ,  $\text{O}_2$ ) individually.

The first term represents the diffusive flux, where  $D_i$  is the diffusion coefficient,  $c_i$  is the species concentration. The second term, which represents electric migration, consists of the charge

Código de campo cambiado



number  $z_i$ , the species mobility  $u_{mi}$ , and the electrolyte potential  $\Phi_{l,e}$ . In the convective flux, represented by the third term,  $u$  is the velocity vector.

The mobility of ions is determined by Nernst- Einstein relation, as follows:

$$u_{mi} = \frac{D_i}{RT} \quad (3)$$

where  $R$  is the universal gas constant and  $T$  is the temperature in K.

The charge balance inside the electrolyte channels is derived from Faraday's law:

$$\nabla \cdot \mathbf{i}_{l,e} = F \sum_i z_i R_i \quad (4)$$

where  $i_{l,e}$  is the electrolyte current density. Since there is no  $R_i$  term inside the electrolyte channels, the charge conservation reduces to:

$$\nabla \cdot \mathbf{i}_{l,e} = 0 \quad (5)$$

The electrolyte current density is given as follows:

$$\mathbf{i}_{l,e} = F \sum_i z_i \left( -D_i \nabla c_i - z_i u_{mi} F c_i \nabla \Phi_{l,e} \right) \quad (6)$$

Inside the electrolyte channels, the electroneutrality condition prevails as described by the following equation:

$$\sum_i z_i c_i = 0 \quad (7)$$

For the incompressible laminar fluid flow inside the electrolyte channels, the Navier-Stokes along with the continuity equations are used to describe the momentum transport and mass conservation as follows:

$$\mathbf{u} \cdot \nabla \mathbf{u} - \nu \nabla^2 \mathbf{u} + \frac{1}{\rho} \nabla p = 0 \quad (8)$$

$$\nabla \cdot \mathbf{u} = 0 \quad (9)$$

where  $\nu$  is the kinematic viscosity.

#### Membrane

Protons are transferred through the membrane from the anode to the cathode side to complete the cathodic reactions. In the Nafion 117 membrane the negative sulfonic ions are fixed in the polymer matrix, implying that the concentration is constant, and the only positive ion present is  $\text{H}^+$ .<sup>37 38</sup> Therefore, due to electroneutrality, the proton flux is given by:

$$N_{\text{H}^+} = -z_i u_{mi} F c_i \nabla \Phi_{l,m} \quad (10)$$

and from Ohm's law

$$\mathbf{i}_{l,m} = -\sigma_{l,m} \nabla \Phi_{l,m} \quad (11)$$

where,  $\sigma_{l,m}$  is the membrane electric conductivity.

#### Cathode and Anode catalyst layers

The probable reaction pathway of  $\text{CO}_2$  electrochemical reduction to  $\text{CH}_3\text{OH}$  involves intermediate species formation in several steps. Since the reduction requires 6 electrons, the

reaction is considered to be kinetically slow and requires very selective catalysts.<sup>7</sup> This work only considers the CO<sub>2</sub> dissolved in the electrolyte and uses its concentration in the kinetic rate equations. The rates of the electrochemical reactions follow Butler-Volmer equation.<sup>39</sup>

As the reaction of CO<sub>2</sub> electro-reduction is limited by mass transfer of CO<sub>2</sub> from the liquid bulk to the surface of the electrode<sup>30</sup>, the concentration-dependent Butler-Volmer equation form was used at cathode surface for both CH<sub>3</sub>OH and CO formation reactions. This form is given as:

$$i_{loc} = k_i \left[ C_R \exp\left(\frac{\alpha_a F \eta}{RT}\right) - C_o \exp\left(\frac{-\alpha_c F \eta}{RT}\right) \right] \quad (12)$$

where,  $i_{loc}$  is the local charge transfer current density for the reaction,  $k_i$  is a kinetic pre-exponential parameter for reactions 1 and 2,  $C_R$  and  $C_O$  are reduced and oxidized species expressions respectively,  $\alpha_a$  and  $\alpha_c$  are anodic and cathodic charge transfer coefficients and  $\eta$  is the overpotential.

For Reactions 1 and 2 at the cathode side,  $C_R$  is set to 0 and  $C_O$  is made a linear function of the concentration of CO<sub>2</sub> and H<sup>+</sup>, both of which are reactants in the two reactions. The final form for the current density at the cathode is as follows:

$$i_{loc} = -k_i \frac{c_{CO_2} c_{H^+}}{c_{ref}^2} \exp\left(\frac{-\alpha_c F \eta}{RT}\right) \quad (13)$$

where  $c_{ref}$  is the reference concentration taken arbitrarily as 31.62 mol/m<sup>3</sup>. This empirical expression accounts for the concentration of the reactants at the cathode interface hindered by mass transfer limitations. The pre-exponential constant in Equation 13 cannot be compared to the exchange current density unless the constant is multiplied by the average concentration of CO<sub>2</sub> and H<sup>+</sup> along the surface of the cathode.

The overpotential is computed from the following equation:<sup>39</sup>

$$\eta = \Phi_{cath,ext} - \Phi_{l,e} - E_{eq} \quad (14)$$

where  $\Phi_{cath, ext}$  is the applied cathode potential,  $\Phi_{l,e}$  is the electrolyte potential and  $E_{eq}$  is the equilibrium potential of each reaction.

As an aqueous electrolyte is used, the water electrolysis is independent of  $H^+$  and  $OH^-$  ions concentrations.<sup>8</sup> The local current density for water reduction is therefore described by the linear Butler Volmer equation:

$$i_{loc} = k \frac{(\alpha_a + \alpha_c)F\eta}{RT} \quad (15)$$

The reactions source/sink term  $R_i$  of equation 1 at the cathode layer for reactions 1, 2 and 3 is given by:

$$R_i = \frac{\nu_i i_{loc}}{n_i F} \quad (16)$$

where  $\nu_i$  is the stoichiometric coefficient of the species in the reaction and  $n_i$  is the number of participating electrons.

The water oxidation taking place at the anode side is also described by linear Butler-Volmer equation:

$$i_{loc} = k \frac{(\alpha_a + \alpha_c)F\eta}{RT} \quad (17)$$

$\eta$  is the overpotential of the water oxidation reaction and is calculated by the following equation:

$$\eta = \Phi_{anode, ext} - \Phi_{l,e} - E_{eq} \quad (18)$$

where  $\Phi_{anode, ext}$  is the applied anode potential,  $\Phi_{l,e}$  is the electrolyte potential and  $E_{eq}$  is the equilibrium potential of the water oxidation reaction.

### Boundary conditions

#### Membrane-free electrolyte boundary conditions

The normal electrolyte current density is equal to the current density in the membrane:

$$\mathbf{n} \cdot \mathbf{i}_{l,e} = \mathbf{n} \cdot \mathbf{i}_{l,m} \quad (19)$$

Proton flux is related to the current density by Faraday's law:

$$\mathbf{n} \cdot \mathbf{N}_{H^+,e} = \mathbf{n} \cdot \frac{\mathbf{i}_{l,m}}{F} \quad (20)$$

The membrane potential is related to the electrolyte potential by Donnan potential shift present due to the difference in the concentration of  $H^+$  ion in the membrane and the two electrolytes<sup>38,40</sup>:

$$\Phi_{l,m} = \Phi_{l,e} + \frac{RT}{F} \ln \left( \frac{a_{H^+,m}}{a_{H^+,e}} \right) \quad (21)$$

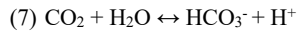
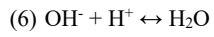
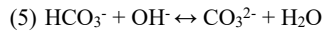
where  $a_{H^+,m}$  is the permeable ion, proton, activity in the membrane, and  $a_{H^+,e}$  is the proton activity in the free electrolyte. Due to the low concentration of ions, activities are replaced by corresponding concentrations. At the interface between electrolyte and membrane, the proton concentration is bound to be equal to the fixed charge site concentration in the membrane.<sup>37</sup>

Figure 2 sums up the governing equations in each modeled domain in the cell and the boundary conditions.

[FIGURE 2]

Inlet conditions (catholyte and anolyte channels)

The dissolution of the CO<sub>2</sub> in the aqueous electrolyte solution of potassium bicarbonate results in various reactions occurring inside this carbonate/bicarbonate system as shown below:



The previous acid-base reactions are fast enough so they are considered as equilibrium reactions inside the electrolyte domains <sup>21</sup>. This equilibrium condition balances the concentrations of H<sup>+</sup> ions and CO<sub>2</sub> in the electrolyte solution at any position. For instance, when the concentration of CO<sub>2</sub> decreases at the cathode due to its consumption, it is instantly produced by Reaction 7 to maintain the equilibrium condition. Likewise, when the H<sup>+</sup> is consumed at the cathode, it is at once produced by Reactions 6 and 7 to retrieve the equilibrium state, which is governed by the mass balance and the electroneutrality conditions.

The corresponding equilibrium constants are defined as:

$$K_1 = \frac{c_{\text{CO}_3^{2-}}}{c_{\text{OH}^-} c_{\text{HCO}_3^-}} = 4.66 \text{ m}^3/\text{mol} \quad (22)$$

$$K_w = c_{\text{H}^+} c_{\text{OH}^-} = 1\text{E}8 \text{ m}^6/\text{mol}^2 \quad (23)$$

$$K_2 = \frac{c_{HCO_3^-} c_{H^+}}{c_{CO_2(L)}} = 4.44E-4 \text{ mol/m}^3 \quad (24)$$

The values for these equilibrium constants were obtained from the work of Gupta<sup>41</sup> for the absorption of CO<sub>2</sub> in 0.5 M solution of KHCO<sub>3</sub> at 25 °C.

To get the inlet concentrations of the different species in the electrolyte, we used the equilibrium constraints along with the carbon balance and electroneutrality condition as described in the following equations:

$$c_{CO_3^{2-}} = K_1 c_{HCO_3^-} c_{OH^-} \quad (25)$$

$$K_w c_{H^+} c_{OH^-} = 1 \quad (26)$$

$$c_{H^+} c_{HCO_3^{2-}} = K_2 c_{CO_2(L)} \quad (27)$$

$$c_{CO_2(dis)} + c_{HCO_3^-} = c_{CO_2(L)} + c_{HCO_3^-} + c_{CO_3^{2-}} \quad (28)$$

$$c_{K^+} + c_{H^+} = 2c_{CO_3^{2-}} + c_{HCO_3^-} + c_{OH^-} \quad (29)$$

To solve these equations for the inlet concentrations, the initial amount of CO<sub>2</sub> dissolved,  $c_{CO_2(dis)}$  in the electrolyte solution is needed. Before the experiment, the 0.5 M solution of KHCO<sub>3</sub> was saturated with CO<sub>2</sub> by continuous bubbling for 20 minutes<sup>30</sup>. The CO<sub>2</sub> dissolution results in reactions 5-7 listed above, which means that the CO<sub>2</sub> concentration in the liquid bulk will differ from the initial dissolved amount due to Reaction 7.

The amount of CO<sub>2</sub> initially dissolved in the 0.5 M KHCO<sub>3</sub> solution can be predicted by the following relation:<sup>42-44</sup>

$$\log\left(\frac{c_{Go}}{c_G}\right) = \sum (h_i + h_g) c_i \quad (30)$$

Where,  $\frac{c_{Go}}{c_G}$  is the ratio of the gas solubility in water to that in the salt solution.

$h_i$  and  $h_G$  are respectively ion specific and gas specific parameters, mol/l

$c_i$  is the concentration of ion i, mol/l

The values of  $h_i$  and  $h_G$  were obtained from the work of Schumpe<sup>43</sup> and are 0.0959, 0.1372 and - 0.0183 mol/l for  $K^+$ ,  $HCO_3^-$  and  $CO_2$  respectively. Using these values and substituting  $c_i$  as 0.5 mol/l, the ratio  $c_{Go}/c_G$  is found to be 1.2538. The solubility of  $CO_2$  in water,  $c_{Go}$ , at 298 K is 0.03395 mol/l.<sup>45</sup> Therefore, the value of  $c_G$ , which is the  $c_{CO_2(dis)}$ , is 0.027 mol/l.

Table 1 shows the base case parameters used in the model.

**[TABLE 1]**

## Results and Discussion

### Numerical solution

The previous governing equations were solved with COMSOL Multiphysics® 5.1 using its pre-programmed module for batteries and fuel cells. Tertiary and secondary current distribution interfaces were coupled to solve for the species concentrations, electrolyte potential and membrane potential across the cell. A user defined mesh was used with mapped distributions in the catholyte, membrane and anolyte domains. The number of elements was varied in these three domains according to the precision required in the solution. The final mesh contained 1400 domain elements and 212 boundary elements. The model was solved with COMSOL® built-in direct solver MUMPS with 68346 degrees of freedom.

### Model validation and parameter fitting



The different kinetic parameters of the electrochemical reactions involved were obtained by parameter fitting using the optimization built-in module in COMSOL®. The optimization goal was to decrease the discrepancy between the experimental and modeled current density values by varying the kinetic parameters of the kinetic rate equations.

The following table shows the different kinetic parameters obtained from the optimization of the model to fit the experimental results.

[TABLE 2]

To perform an order-of-magnitude comparison of the values obtained for the pre-exponential kinetic parameter with the exchange current density reported in the literature<sup>46,47</sup> for the CO<sub>2</sub> electrochemical reduction, the obtained pre-exponential parameter has to be multiplied by the average concentration of CO<sub>2</sub> and H<sup>+</sup> because these concentrations were used in the rate equation (Eq. 13). For the base case, the use of the average concentrations, which are 0.27727 and 2.9E-4 mol/m<sup>3</sup>, for CO<sub>2</sub> and H<sup>+</sup> respectively, result in an average exchange current densities of 9.65 and 0.00804 A/m<sup>2</sup>, for the reduction of CO<sub>2</sub> to methanol and CO respectively. The value of the average exchange current density for methanol production obtained by this method is high. It must be stressed that these values are empirical in the sense that they fit the data well but they cannot be represented as exchange current densities due to the simplifications made in the representation of the cathode interface and the mass-transfer behavior at the cathode surface as well as the arbitrary nature of kinetic rate equation (Eq. 13). The same discussion also applies to the hydrogen and oxygen evolution reactions.

The model is then validated by comparing the experimental results of applied potential variations following the procedure and system from a previous work<sup>30</sup> against the results predicted by the model. The modeled results agree with the experimental ones with minor error. The deviation between the modeled and experimental total current densities is calculated using the relative error root mean square and is found to be equal to 20.2%. Figure 3 shows a comparison between the simulated and the experimental values of the current density as a function of the applied potential.

[FIGURE 3]

The fit between the model and the experimental results is good around cathode potentials between -1.3 V and -1.5 V, corresponding to cell potentials of -2.33 and -2.53 V, where the cell would be normally operated as CH<sub>3</sub>OH formation is favorable. At more negative cathode potential (-1.7 V), the current density increases which implies a higher concentration of reduced species corresponding to the combination of different electrochemical reactions at the cathode. However, this increased formation of reduced species hinders the CH<sub>3</sub>OH production as it is shown experimentally that the outlet CH<sub>3</sub>OH concentration decreases at this voltage.

## Base case results

### Species production at the cathode

CH<sub>3</sub>OH, H<sub>2</sub> and CO are produced at the cathode with different rates depending on the parameters in their kinetic rate equations. Figure 4 show the production fluxes of these different species across the cathode length. The fluxes of CH<sub>3</sub>OH and the CO are function of the concentration of the reactants at the surface of the cathode. At the entrance of the cell, CH<sub>3</sub>OH and CO are produced by their respective reactions once the catholyte flows in. This production escalates until

it reaches a maximum value at the beginning of the cathode side and then falls rapidly due to a gradual decrease in the mass transport of  $\text{CO}_2$  and  $\text{H}^+$  demonstrated in subsequent figures. The production of hydrogen from water has a similar reduction potential as the formation of  $\text{CH}_3\text{OH}$  from  $\text{CO}_2$ . The provided potential to the system could be partially consumed by water reduction rather than  $\text{CO}_2$  reduction as is evident by Figure 4. As the water electrolysis at the cathode is independent on the concentration of  $\text{H}^+$ ,<sup>27</sup>  $\text{H}_2$  continues to be produced across the cathode length until the outlet of the cell in agreement with a previous study.<sup>29</sup>

[FIGURE 4]

#### Current density at the cathode

Figure 5 shows the current density at the cathode. As depicted, the current density starts at its maximum value at the inlet of the cell due to the instant reactions occurring at the cathode surface producing different species. Similar to the pattern of the  $\text{CH}_3\text{OH}$  and  $\text{CO}$  production, the current density begins to decrease as the rate of the reactions declines due to the reactants expeditious consumption. After reaching a minimum value, the current density slightly increases again then stabilizes for the remaining part of the cell due to the dominance of the HER partial current density, also shown in Figure 5. The HER partial current density dominates the shape of the total current density from a cathode length around 5 mm till the cell exit.

[FIGURE 5]

#### Electrolyte potential

Figure 6 shows the distribution of the electrolyte potential across the width of the cell. The Donnan potential shifts around the boundaries of the membrane are clearly visible in the figure.

While Figure 7 shows a 2D surface plot for the electrolyte potential variation in the catholyte. The plot shows a high **potential** at the inlet of the cell due to the high rate **of reactions**. As the **rate of reactions** begins to decline, the electrolyte potential decreases.

[FIGURE 6]

[FIGURE 7]

#### Reactants transport

Figure 8 shows the  $\text{CO}_2$  and  $\text{H}^+$  total normal fluxes at the cathode. The total flux for  $\text{CO}_2$  is the diffusive flux, while the total flux for  $\text{H}^+$  is the diffusive and the electrophoretic fluxes. The fluxes begin with a high value at the inlet of the cell then starts to fall as the rate of the proceeding reactions is greater than the mass transfer rate. The decline rate of  $\text{CO}_2$  flux is greater than that of  $\text{H}^+$  flux illustrating that the reaction rate is mainly hindered by the mass transfer limitations of  $\text{CO}_2$  to the cathode in agreement with previous studies.<sup>16,30,48</sup> This decline can also be explained by the competition of the **HER** in the available catalytic surface at the applied potential.

[FIGURE 8]

#### Electrolyte Flowrate effect

Typically, the increase in the flowrate results in better mixing and enhanced mass transfer characteristics for the reactants close to the surface of the electrode. This convective mass-transfer enhancement would lead to bringing the reactants faster to where they react and, thus, improves the rate of reaction. In our model, however, the fluid is assumed to have a laminar velocity profile in the longitudinal direction with no velocity components in the horizontal

direction. Thus, our base-case model does not capture the effect of the velocity on the improvement of mass-transfer. The laminar velocity profile assumption can be relaxed in different ways. We used a simple first-order relaxation step to show qualitatively that with proper fluid flow model, the base-case model can be enhanced to fully capture the effect of the flow pattern variation on the current density profile. The simple improvement was the use of constant velocity profile at the inlet of the cell. Now, there will be both longitudinal and horizontal components of the velocity at the entrance zone of the cell until the fluid reaches a parabolic velocity profile with zero horizontal component. This entrance effect will in turn has its impact on the mass transfer behavior. The increase in velocity will result in enhanced transport of the reactants to the electrode surface. Figure 9 shows the flowrate variation effect on the current density from the model vs. the experiments at the same base case parameters and an applied cathode potential of -1.3 V.

[FIGURE 9]

The modeling results agree with the experimental ones with an average error of 12%. The results show that the electro-reduction of CO<sub>2</sub> can be slightly improved by increasing the electrolyte flowrate.<sup>30</sup> The marginal increase in the current density may indicate that the reaction is primarily limited by the mass transfer at the electrode surface. A second-order relaxation step would be to include the entrance zone before the actual cell to fully understand the impact of the flow pattern. However, this second step has not been attempted.

Figure 10 below depicts the flowrate variation effect on both the average CH<sub>3</sub>OH concentration and the faradaic efficiency (FE) of the CH<sub>3</sub>OH formation. There is an obvious tradeoff between the two parameters; while the FE increases with increasing the flowrate, the average CH<sub>3</sub>OH

concentration decreases in agreement with previous study.<sup>30</sup> Using a low electrolyte flowrate gives a concentrated product with a much lower FE than a higher flowrate. A balance is required between these two parameters to reach optimum operating conditions.

[FIGURE 10]

#### Membrane effect

The  $\text{CH}_3\text{OH}$  produced at the cathode surface flows out of the cell with the flowing electrolyte by convection. As the electrolyte is flowing in the longitudinal direction, the only way for  $\text{CH}_3\text{OH}$  to be transported horizontally across the cell in the model is by diffusion. The lateral diffusion term in the governing equation for the transport of  $\text{CH}_3\text{OH}$  diminishes in comparison with the longitudinal convection term. In particular, the longitudinal convective flux is two orders of magnitude higher than the lateral diffusive flux for  $\text{CH}_3\text{OH}$ , as shown in Figure 11.

[FIGURE 11]

Figure 11 shows the  $\text{CH}_3\text{OH}$  convective and diffusive fluxes across part of the cathode chamber. The discrepancy is clear as the diffusive flux is almost insignificant compared to the convective one. Therefore, the flow pattern of the  $\text{CH}_3\text{OH}$  produced suggests that it is unlikely for the  $\text{CH}_3\text{OH}$  to be transported to the anodic compartment where it could be re-oxidized. Based on this, an experiment was conducted without the membrane at the same base case conditions. The results showed that the rate of  $\text{CH}_3\text{OH}$  formation is only reduced by 28% while the current density, which represents the rate of electrochemical reactions, increased by approximately 69%. This can be explained by the fact that removing the membrane removes the resistance it imposes, hence, the efficiency of electrical energy consumption increases. This result is in agreement with a previous study which compared the performance of a filter press cell with various types of

membranes vs. the no membrane cell.<sup>49</sup> The production rate of CH<sub>3</sub>OH probably decreases due to the excessive formation of other byproducts. Taking this into consideration, a more effective design of the cell could be adopted in the scale up of the process, such as for example using alternative high conductive membrane materials.

#### Electrochemical characteristics

As the applied cathode potential shifts from -1.3 V to -1.5 V, the partial current density for HER increases by more than 47%. This agrees with previous studies that showed that for more negative cathode potential than -1.3 V (vs. Ag/AgCl), significant hydrogen evolution was taking place at the cathode.<sup>30</sup>

Figure 12 shows a distribution for the partial current densities of CH<sub>3</sub>OH and HER and the FE for CH<sub>3</sub>OH at different cell potentials. The HER partial current density accounts for most of the total current density value and the highest FE reached for the CH<sub>3</sub>OH formation is around 17.3% at a cathode potential of -1.3 V. The partial current density of HER increases almost linearly with the total current density increase while the CH<sub>3</sub>OH partial current density slightly decreases along with the FE. This pattern agrees with previous findings recommending continuous research for more selective catalysts that suppress the H<sub>2</sub> formation favoring the CH<sub>3</sub>OH.<sup>6,7,30,50</sup>

[FIGURE 12]

### **Conclusion**

This work presented a 2D model for the electrochemical reduction of CO<sub>2</sub> to CH<sub>3</sub>OH in a microfluidic cell. The model takes into account the significant physical phenomena occurring inside the cell as species and charge transport, charge conservation, fluid flow and electrode

kinetics. The model is fitted to experimental results to obtain the different kinetic parameters. Experimental data are also used to validate the model with an average error of 20.2%. Results showed the effect of mass transfer limitations on the rate of the CH<sub>3</sub>OH formation reaction which suggests the need to improve the CO<sub>2</sub> transport to the cathode. The results also illustrated the H<sub>2</sub> formation dominance over the CH<sub>3</sub>OH production. The flowrate variation effect on the performance of the microfluidic cell is shown. Based on the Nafion membrane effect studied, the results show that more conductive membrane materials could be employed to decrease the potential losses across the cell and therefore increase the overall efficiency of the process. To the best of our knowledge, this is the first mathematical model developed for the electrochemical reduction of CO<sub>2</sub> to alcohols. Hence, it opens a new line for further improvements to include the porous flow of CO<sub>2</sub> gas through the gas diffusion electrodes and to increase the number of reactions occurring to mirror the actual performance with the aim of the process scale up.

### Nomenclature

$a_{H^+,e}$	Activity of H <sup>+</sup> in electrolyte
$a_{H^+,m}$	Activity of H <sup>+</sup> in membrane
$c_i$	Concentration of species i, mol/m <sup>3</sup>
$c_{CO_2(dis)}$	Initial dissolved amount of CO <sub>2</sub> , mol/m <sup>3</sup>
$c_{CO_2(L)}$	Concentration of CO <sub>2</sub> in the liquid bulk, mol/m <sup>3</sup>
$c_G$	Gas solubility in salt solution, mol/l
$c_{Go}$	Gas solubility in water, mol/l
$C_O$	Oxidized species concentration expression
$C_R$	Reduced species concentration expression
$D_i$	Diffusion coefficient of species i, m <sup>2</sup> /s
$E_{eq}$	Equilibrium potential of half-cell reaction, V
$F$	Faraday's constant
$FE$	Faradaic efficiency



$h_G$	Gas specific parameter, mol/l
$h_i$	Ion specific parameter, mol/l
$i_{o,i}$	Exchange current density of reaction i, A/m <sup>2</sup>
$i_{l,e}$	Current density in electrolyte, A/m <sup>2</sup>
$i_{l,m}$	Current density in membrane, A/m <sup>2</sup>
$i_{loc}$	Local charge transfer current density, A/m <sup>2</sup>
$k_i$	Kinetic rate parameter, A/m <sup>2</sup>
$n$	Number of participating electrons in reaction
$N_i$	Molar flux of species i, mol/m <sup>2</sup> s
$R$	Universal gas constant
$R_i$	Reaction source/sink term
$T$	Temperature, K
$u$	Velocity of electrolyte, m/s
$u_{mi}$	Mobility of ion i, s mol/kg
$z_i$	Charge number of ion i
$\alpha_a$	Anodic charge transfer coefficient
$\alpha_c$	Cathodic charge transfer coefficient
$\eta$	Overpotential, V
$\nu$	Kinematic viscosity, m <sup>2</sup> /s
$\nu_i$	Stoichiometric coefficient of species i
$\sigma_{l,m}$	Membrane electric conductivity, S/m
$\Phi_{anode,ext}$	Applied anode potential, V
$\Phi_{cath,ext}$	Applied cathode potential, V
$\Phi_{l,e}$	Electrolyte potential, V
$\Phi_{l,m}$	Membrane potential, V

## References

1. Edenhofer O, Pichs-Madruga R, Sokona Y, et al. Technical Summary. In: *Climate Change 2014: Mitigation of Climate Change. Contribution of Working Group III to the Fifth Assessment Report of the Intergovernmental Panel on Climate Change*. Cambridge University Press, Cambridge, United Kingdom and New York, NY, USA; 2014.
2. Albo J, Luis P, Irabien A. Absorption of coal combustion flue gases in ionic liquids using different membrane contactors. *Desalin Water Treat*. 2011;27(1-3):54-59. doi:DOI 10.5004/dwt.2011.2050.
3. Yang H, Xu Z, Fan M, et al. Progress in carbon dioxide separation and capture: A review. *J Environ Sci*. 2008;20(1):14-27. doi:10.1016/S1001-0742(08)60002-9.
4. Bachu S, Celia MA. Assessing the potential for CO<sub>2</sub> leakage, particularly through wells, from geological storage sites. *Carbon Sequestration Its Role Glob Carbon Cycle*. 2009;203-216. doi:10.1029/2005GM000338.
5. Markewitz P, Kuckshinrichs W, Leitner W, et al. Worldwide innovations in the development of carbon capture technologies and the utilization of CO<sub>2</sub>. *Energy Environ Sci*. 2012;5(6):7281. doi:10.1039/c2ee03403d.
6. Ganesh I. Conversion of carbon dioxide into methanol – a potential liquid fuel: Fundamental challenges and opportunities (a review). *Renew Sustain Energy Rev*. 2014;31:221-257. doi:10.1016/j.rser.2013.11.045.
7. Albo J, Alvarez-Guerra M, Castaño P, Irabien a. Towards the electrochemical conversion of carbon dioxide into methanol. *Green Chem*. 2015. doi:10.1039/C4GC02453B.
8. Wu K, Birgersson E, Kim B, Kenis PJ a., Karimi I a. Modeling and Experimental Validation of Electrochemical Reduction of CO<sub>2</sub> to CO in a Microfluidic Cell. *J*

*Electrochem Soc.* 2014;162(1):F23-F32. doi:10.1149/2.1021414jes.

9. Yamamoto T, Tryk DA, Fujishimal A, Ohata H. Production of syngas plus oxygen from CO<sub>2</sub> in a gas-diffusion electrode-based electrolytic cell. *Electrochim Acta*. 2002;47(20):3327-3334. doi:10.1016/S0013-4686(02)00253-0.
10. Agarwal AS, Zhai Y, Hill D, Sridhar N. The electrochemical reduction of carbon dioxide to formate/formic acid: Engineering and economic feasibility. *ChemSusChem*. 2011;4:1301-1310. doi:10.1002/cssc.201100220.
11. Alvarez-Guerra M, Del Castillo A, Irabien A. Continuous electrochemical reduction of carbon dioxide into formate using a tin cathode: Comparison with lead cathode. *Chem Eng Res Des*. 2014;92(4):692-701. doi:10.1016/j.cherd.2013.11.002.
12. Merino García I, Albo J, Irabien A. Productivity and selectivity of gas phase CO<sub>2</sub> electroreduction to methane at Cu nanoparticle-based electrodes. *Energy Technol*. 2016. doi:10.1002/ente.201600616.
13. Kaneco S, Hiei NH, Xing Y, et al. Electrochemical conversion of carbon dioxide to methane in aqueous NaHCO<sub>3</sub> solution at less than 273 K. *Electrochim Acta*. 2002;48:51-55. doi:10.1016/S0013-4686(02)00550-9.
14. Kaneco S, Iiba K, Hiei N, Ohta K, Mizuno T, Suzuki T. Electrochemical reduction of carbon dioxide to ethylene with high Faradaic efficiency at a Cu electrode in CsOH/methanol. *Electrochim Acta*. 1999;44(x):4701-4706. doi:10.1016/S0013-4686(99)00262-5.
15. Ogura K. Electrochemical reduction of carbon dioxide to ethylene: Mechanistic approach. *J CO<sub>2</sub> Util*. 2013;1:43-49. doi:10.1016/J.jcou.2013.03.003.
16. Albo J, Irabien A. Cu<sub>2</sub>O-loaded gas diffusion electrodes for the continuous

electrochemical reduction of CO<sub>2</sub> to methanol. *J Catal.* 2016;343:232-239.

doi:10.1016/j.jcat.2015.11.014.

17. Albo J, Vallejo D, Beobide G, Castillo O, Castano P, Irabien A. Copper-Based Metal-Organic Porous Materials for CO<sub>2</sub> Electrocatalytic Reduction to Alcohols. *ChemSusChem.* 2016;1-11. doi:10.1002/cssc.201600693.
18. Albo J, Beobide G, Castaño P, Irabien A. Methanol electrosynthesis from CO<sub>2</sub> at Cu<sub>2</sub>O/ZnO prompted by pyridine-based aqueous solutions. *J CO<sub>2</sub> Util.* 2017;18:164-172. doi:10.1016/j.jcou.2017.02.003.
19. Goeppert A, Czaun M, Jones J-P, Surya Prakash GK, Olah G a. Recycling of carbon dioxide to methanol and derived products - closing the loop. *Chem Soc Rev.* June 2014. doi:10.1039/c4cs00122b.
20. Olah G a., Goeppert A, Prakash GKS. Chemical recycling of carbon dioxide to methanol and dimethyl ether: From greenhouse gas to renewable, environmentally carbon neutral fuels and synthetic hydrocarbons. *J Org Chem.* 2009;74:487-498. doi:10.1021/jo801260f.
21. Delacourt C, Ridgway PL, Newman J. Mathematical Modeling of CO<sub>2</sub> Reduction to CO in Aqueous Electrolytes. *J Electrochem Soc.* 2010;157(12):B1902. doi:10.1149/1.3502532.
22. Li H, Oloman C. Development of a continuous reactor for the electro-reduction of carbon dioxide to formate - Part 2: Scale-up. *J Appl Electrochem.* 2007;37(10):1107-1117. doi:10.1007/s10800-007-9371-8.
23. Ni M. An Electrochemical Model for Syngas Production by Co- electrolysis of H<sub>2</sub>O and CO<sub>2</sub>. *J Power Sources.* 2012;202(852):209-216.
24. Ni M. 2D thermal modeling of a solid oxide electrolyzer cell (SOEC) for syngas

production by H<sub>2</sub>O/CO<sub>2</sub> co-electrolysis. *Int J Hydrogen Energy*. 2012;37(8):6389-6399. doi:10.1016/j.ijhydene.2012.01.072.

25. Xie Y, Xue X. Modeling of solid oxide electrolysis cell for syngas generation with detailed surface chemistry. *Solid State Ionics*. 2012;224:64-73. doi:10.1016/j.ssi.2012.07.015.
26. Luo Y, Shi Y, Li W, Cai N. Comprehensive modeling of tubular solid oxide electrolysis cell for co-electrolysis of steam and carbon dioxide. *Energy*. 2014;70(April 2016):420-434. doi:10.1016/j.energy.2014.04.019.
27. Whipple DT. Microfluidic Platform For Studying The Electrochemical Reduction of Carbon Dioxide. *J Chem Inf Model*. 2011.
28. Jhong HRM, Ma S, Kenis PJ. Electrochemical conversion of CO<sub>2</sub> to useful chemicals: Current status, remaining challenges, and future opportunities. *Curr Opin Chem Eng*. 2013;2(2):191-199. doi:10.1016/j.coche.2013.03.005.
29. Wang H, Leung DY, Xuan J. Modeling of a microfluidic electrochemical cell for CO<sub>2</sub> utilization and fuel production. *Appl Energy*. 2013;102:1057-1062. doi:10.1016/j.apenergy.2012.06.020.
30. Albo J, Sáez A, Solla-Gullón J, Montiel V, Irabien A. Production of methanol from CO<sub>2</sub> electroreduction at Cu<sub>2</sub>O and Cu<sub>2</sub>O/ZnO-based electrodes in aqueous solution. *Appl Catal B Environ*. 2015;176-177(MAY):709-717. doi:10.1016/j.apcatb.2015.04.055.
31. Kuhl KP, Cave ER, Abram DN, Jaramillo TF. New insights into the electrochemical reduction of carbon dioxide on metallic copper surfaces. *Energy Environ Sci*. 2012;5:7050. doi:10.1039/c2ee21234j.
32. Birgersson E, Noponen M, Vynnycky M. Analysis of a Two-Phase Non-Isothermal Model

for a PEFC. *J Electrochem Soc.* 2005;152(5):A1021. doi:10.1149/1.1877992.

33. Secanell Gallart M. Computational Modeling and Optimization of Proton Exchange Membrane Fuel Cells. *Univ Victoria.* 2007.
34. Um S, Wang C-Y, Chen KS. Computational Fluid Dynamics Modeling of Proton Exchange Membrane Fuel Cells. *J Electrochem Soc.* 2000;147(12):4485-4493. doi:10.1149/1.1394090.
35. Ni M. An electrochemical model for syngas production by co-electrolysis of H<sub>2</sub>O and CO<sub>2</sub>. *J Power Sources.* 2012;202:209-216. doi:10.1016/j.jpowsour.2011.11.080.
36. Wang H, Leung DY, Xuan J. Modeling of an air cathode for microfluidic fuel cells: Transport and polarization behaviors. *Int J Hydrogen Energy.* 2011;36(22):14704-14718. doi:10.1016/j.ijhydene.2011.08.033.
37. Shah AA, Watt-Smith MJ, Walsh FC. A dynamic performance model for redox-flow batteries involving soluble species. *Electrochim Acta.* 2008;53(27):8087-8100. doi:10.1016/j.electacta.2008.05.067.
38. Hosseiny SS. Vanadium Redox Flow Battery. *Batter Fuel Cells Modul COMSOL Model Libr Man.* 2011. doi:10.3990/1.9789036532259.
39. Wang CY. Fundamental models for fuel cell engineering. *Chem Rev.* 2004;104(10):4727-4765. doi:10.1021/cr020718s.
40. Knehr KW, Kumbur EC. Open circuit voltage of vanadium redox flow batteries: Discrepancy between models and experiments. *Electrochem commun.* 2011;13(4):342-345. doi:10.1016/j.elecom.2011.01.020.
41. Gupta N, Gattrell M, MacDougall B. Calculation for the cathode surface concentrations in the electrochemical reduction of CO<sub>2</sub> in KHCO<sub>3</sub> solutions. *J Appl Electrochem.*

2006;36:161-172. doi:10.1007/s10800-005-9058-y.

42. Cents AHG, Brilman DWF, Versteeg GF. Gas absorption in an agitated gas–liquid–liquid system. *Chem Eng Sci.* 2001;56(3):1075-1083. doi:10.1016/S0009-2509(00)00324-9.
43. Schumpe A. The estimation of gas solubilities in salt solutions. *Chem Eng Sci.* 1993;48(1):153-158. doi:10.1016/0009-2509(95)00031-Y.
44. Weisenberger S, Schumpe a. Estimation of gas solubilities in salt solutions at temperatures from 273 K to 363 K. *AIChE J.* 1996;42(1):298-300. doi:10.1002/aic.690420130.
45. Wilhelm E, Battino R, Wilcock RJ. Low-pressure solubility of gases in liquid water. *Chem Rev.* 1977;77:219-262. doi:10.1021/cr60306a003.
46. Prakash GKS, Viva FA, Olah GA. Electrochemical reduction of CO<sub>2</sub> over Sn-Nafion® coated electrode for a fuel-cell-like device. *J Power Sources.* 2013;223:68-73.
47. Kim C, Jeon HS, Eom T, et al. Achieving selective and efficient electrocatalytic activity for CO<sub>2</sub> reduction using immobilized silver nanoparticles. *J Am Chem Soc.* 2015;137(43):13844-13850.
48. Whipple DT, Kenis PJ a. Prospects of CO<sub>2</sub> utilization via direct heterogeneous electrochemical reduction. *J Phys Chem Lett.* 2010;1:3451-3458. doi:10.1021/jz1012627.
49. Garcia-Herrero I, Alvarez-Guerra M, Irabien A. Electrosynthesis of dimethyl carbonate from methanol and CO<sub>2</sub> using potassium methoxide and the ionic liquid [bmim][Br] in a filter-press cell: a study of the influence of cell configuration. *J Chem Technol Biotechnol.* 2014.
50. Sebastián D, Palella A, Baglio V, et al. CO<sub>2</sub> reduction to alcohols in a polymer electrolyte membrane co-electrolysis cell operating at low potentials. *Electrochim Acta.*

2017;241:28-40. doi:10.1016/j.electacta.2017.04.119.

51. Cents AHG, Brilman DWF, Versteeg GF. CO<sub>2</sub> absorption in carbonate/bicarbonate solutions: The Danckwerts-criterion revisited. *Chem Eng Sci.* 2005;60(21):5830-5835. doi:10.1016/j.ces.2005.05.020.
52. Cunningham AB, Lennox JE, Ross RJ. Diffusion coefficients in water at 25 C.

### Figure Captions

Figure 1. Cell configuration used in modeling

Figure 2. The governing equations and the boundary conditions used in the catholyte, the membrane and the anolyte domains.

Figure 3. Comparison between the current density as predicted by the model and experimentally obtained

Figure 4. The production fluxes of the CH<sub>3</sub>OH, H<sub>2</sub>, and CO along the cathode longitudinal surface as predicted by the model

Figure 5. The current density along the surface of the cathode as predicted by the model and the partial current density obtained from the HER.

Figure 6. Electrolyte and membrane potential distribution across the cell

Figure 7. Surface plot of electrolyte potential variation along the cathode compartment

Figure 8. Total normal fluxes of CO<sub>2</sub> and H<sup>+</sup> along the cathode surface

Figure 9. Comparison between the effect of the electrolyte flowrate on the current density as predicted by the model and experimentally obtained

Figure 10. The effect of the electrolyte flowrate on the FE of CH<sub>3</sub>OH and CH<sub>3</sub>OH concentration



Figure 11. The longitudinal convective flux and the lateral diffusive flux of methanol across part of the cathode compartment

Figure 12. The total current density, the  $\text{CH}_3\text{OH}$  partial current density and the HER partial current density versus the applied cathode potential. The curve shows also the effect of the applied cathode potential on the FE of  $\text{CH}_3\text{OH}$

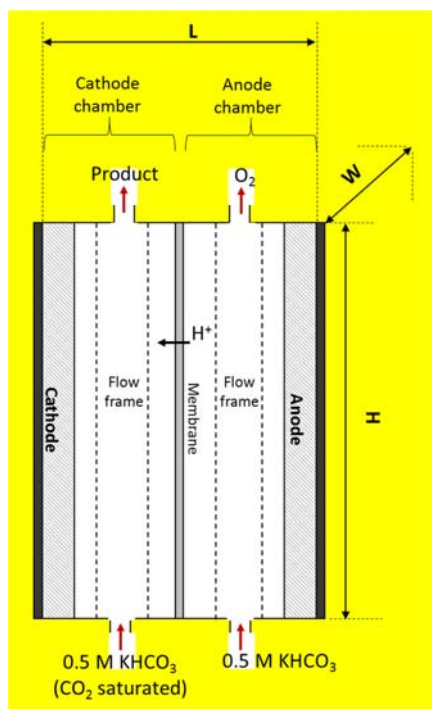


Figure 1. Cell configuration used in modeling

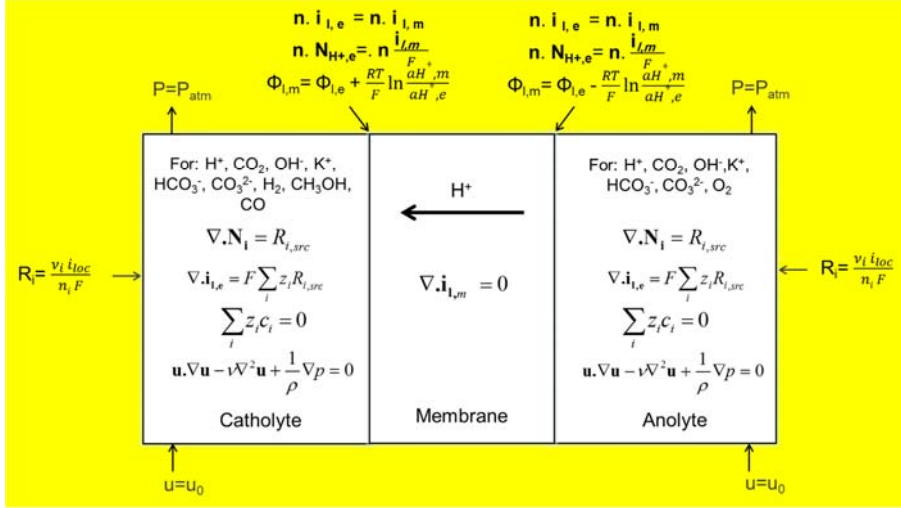


Figure 2. The governing equations and the boundary conditions used in the catholyte, the membrane and the anolyte domains

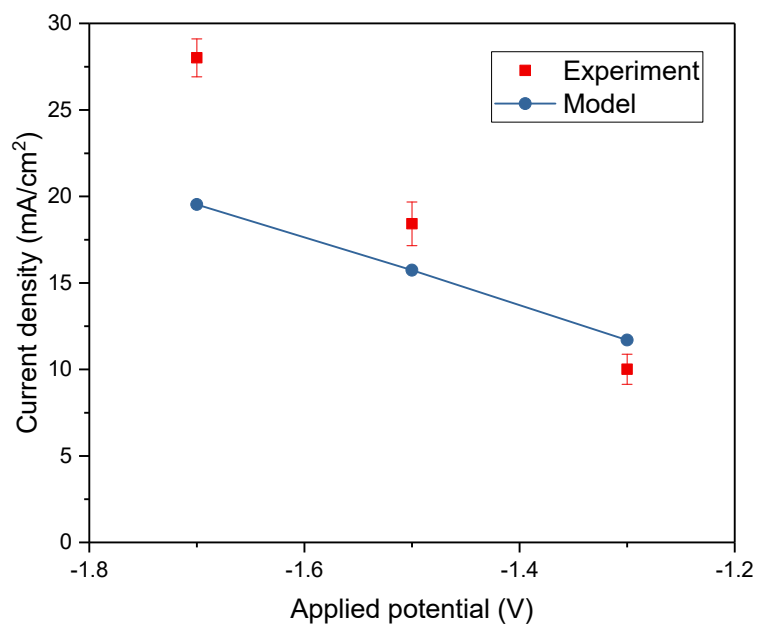


Figure 3. Comparison between the current density as predicted by the model and experimentally obtained

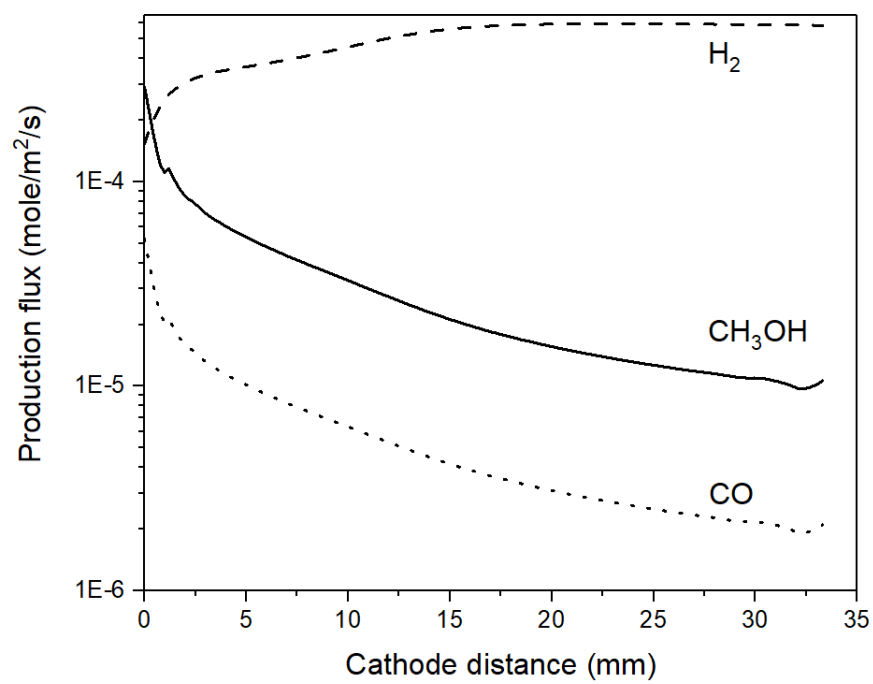


Figure 4. The production fluxes of the CH<sub>3</sub>OH, H<sub>2</sub>, and CO along the cathode longitudinal surface as predicted by the model

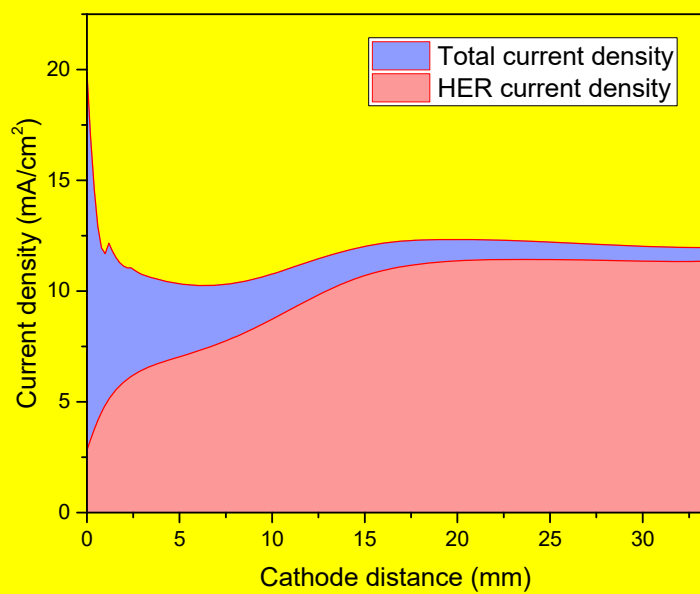


Figure 5. The current density along the surface of the cathode as predicted by the model and the partial current density obtained from the HER.

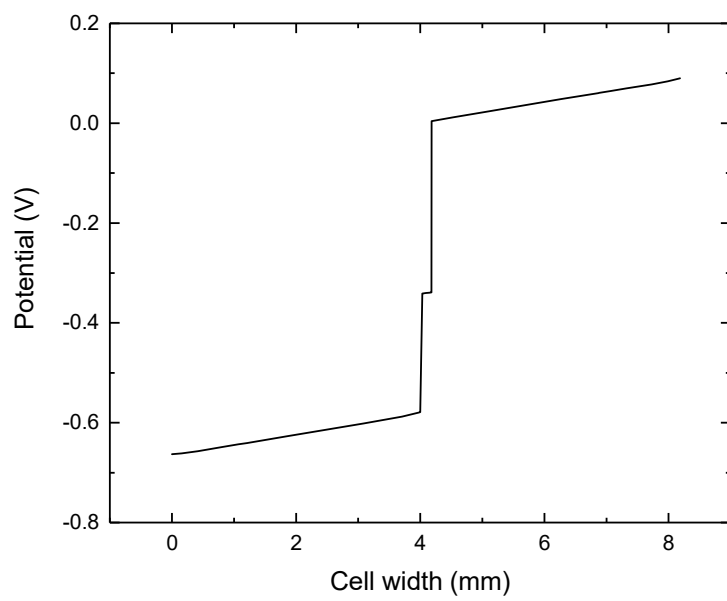


Figure 6. Electrolyte and membrane potential distribution across the cell

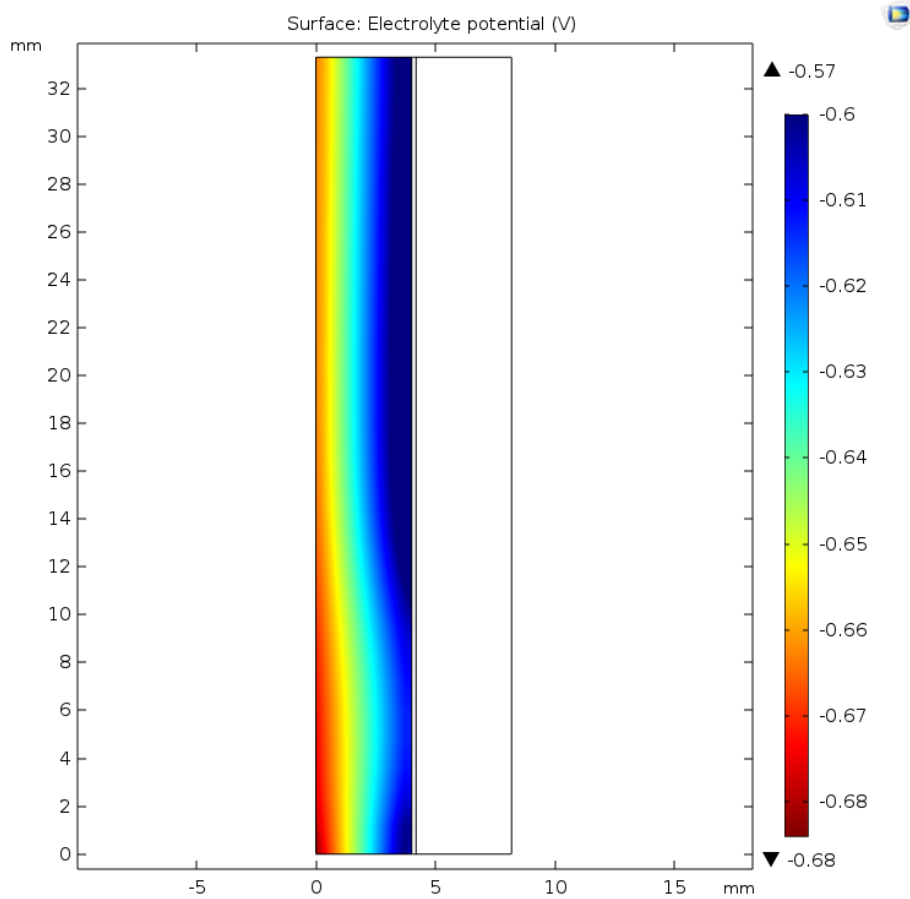


Figure 7. Surface plot of electrolyte potential variation along the cathode compartment



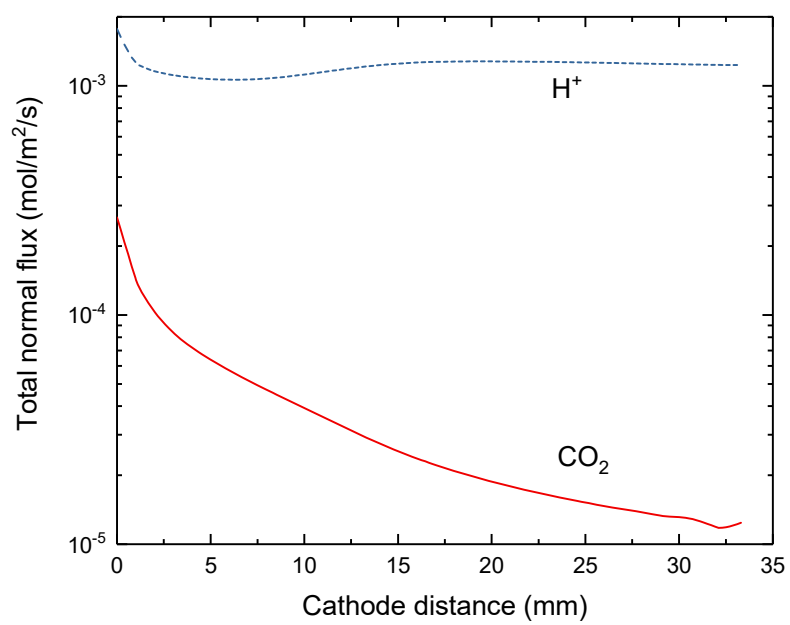


Figure 8. Total normal fluxes of  $\text{CO}_2$  and  $\text{H}^+$  along the cathode surface

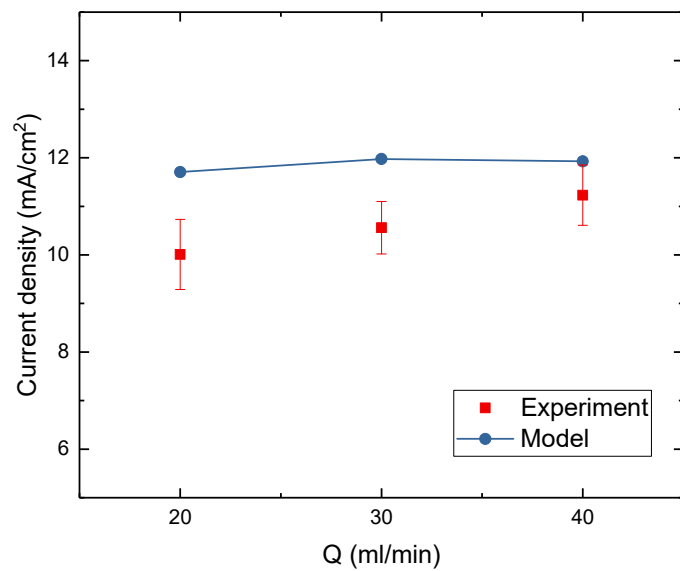


Figure 9. Comparison between the effect of the electrolyte flowrate on the current density as predicted by the model and experimentally obtained

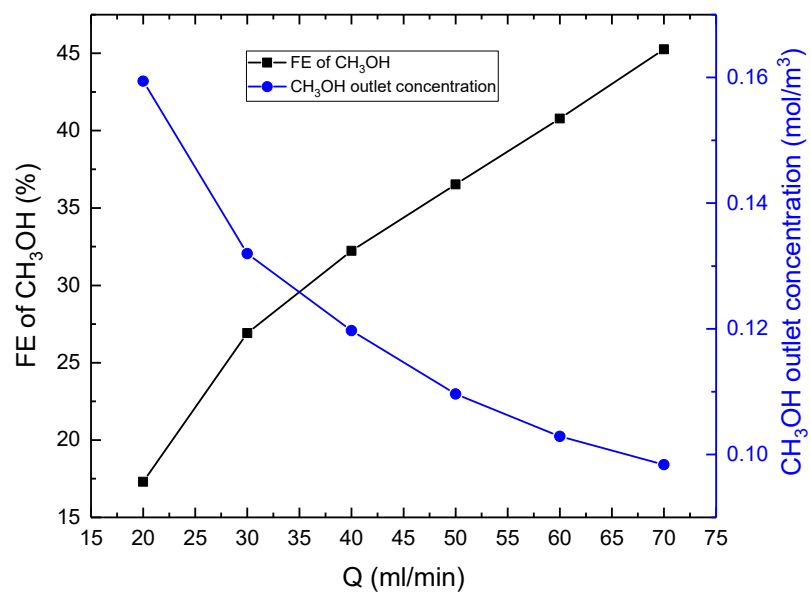


Figure 10. The effect of the electrolyte flowrate on the FE of CH<sub>3</sub>OH and CH<sub>3</sub>OH concentration

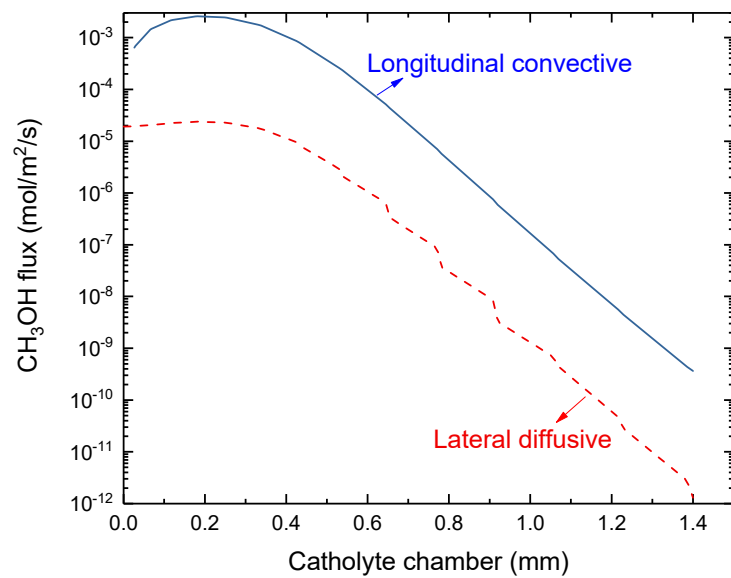


Figure 11. The longitudinal convective flux and the lateral diffusive flux of methanol across part of the cathode compartment

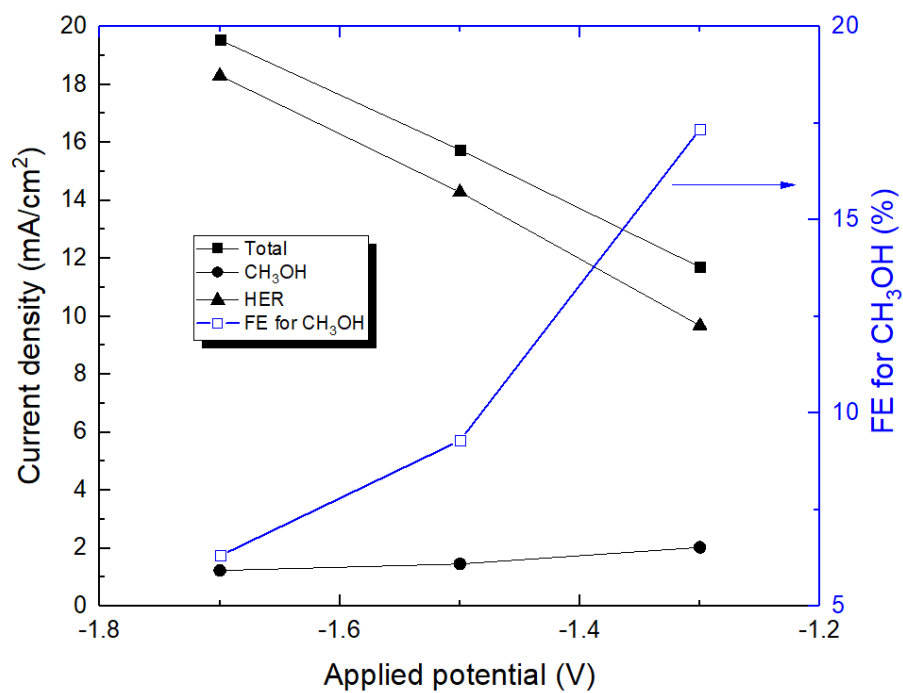


Figure 12. The total current density, the CH<sub>3</sub>OH partial current density and the HER partial current density versus the applied cathode potential. The curve shows also the effect of the applied cathode potential on the FE for CH<sub>3</sub>OH

### **Table Captions**

Table 1. Input model parameters

Table 2. Kinetic parameters for the electrochemical reactions

Table 1. Input model parameters

Parameter	Symbol	Value	Unit	Source
Operating conditions				
Temperature	T	25	°C	30
Pressure	P	1	Bar	
Electrolyte flow rate	Q	20	ml/min	
Cathode applied potential	$\Phi_{\text{cath}}$	-1.3	V	
Anode applied potential	$\Phi_{\text{anode}}$	1.03		
pH	pH	7.6	-	
Cell geometry				
Height	H	34	mm	30
Width	W	34	mm	
Length	L	8.183	mm	
Inlet conditions				
Hydrogen ion concentration	$c_H^+$	2.489E-05	mol/m <sup>3</sup>	Calculated
Hydroxyl ion concentration	$c_{OH}^-$	0.000402		
Bicarbonate ion concentration	$c_{HCO_3}^-$	498.134		
Carbonate ion concentration	$c_{CO_3}^{2-}$	0.932		
Potassium ion concentration	$c_K^+$	500		
CO <sub>2</sub> concentration	$c_{CO_2(L)}$	27.932		
Fluid properties				
Diffusion coefficient of CO <sub>2</sub>	$D_{CO_2}$	1.59E-9	m <sup>2</sup> /s	51
Diffusion coefficient of H <sup>+</sup>	$D_H^+$	9.21E-9		
Diffusion coefficient of CH <sub>3</sub> OH	$D_{CH_3OH}$	1.5E-9		52
Diffusion coefficient of O <sub>2</sub>	$D_{O_2}$	2E-9		
Diffusion coefficient of OH <sup>-</sup>	$D_{OH}^-$	5.17E-9		
Diffusion coefficient of K <sup>+</sup>	$D_K^+$	1.95E-9		
Diffusion coefficient of HCO <sub>3</sub> <sup>-</sup>	$D_{HCO_3}^-$	1.18E-9		51
Diffusion coefficient of CO <sub>3</sub> <sup>2-</sup>	$D_{CO_3}^{2-}$	9.2E-10		
Diffusion coefficient of CO	$D_{CO}$	1E-9		
Diffusion coefficient of H <sub>2</sub>	$D_{H_2}$	2.03E-9		
Membrane properties				
Activity of H <sup>+</sup> in the membrane	$a_H^+$	1200	mol/m <sup>3</sup>	37
Membrane electric conductivity	$\sigma_{l,m}$	10	S/m	

Table 2. Kinetic parameters for the electrochemical reactions

Parameter	Symbol	Value	Unit
CH <sub>3</sub> OH kinetic rate parameter	k <sub>1</sub>	1.2E8	A/m <sup>2</sup>
CO kinetic rate parameter	k <sub>2</sub>	1E5	A/m <sup>2</sup>
HER kinetic rate parameter	k <sub>3</sub>	100	A/m <sup>2</sup>
OER kinetic rate parameter	k <sub>4</sub>	9.4223	A/m <sup>2</sup>